Title: Phytoplankton traits from long-term oceanographic time-series

Running page head: Phytoplankton traits from time-series data

Crispin M Mutshinda[1], Zoe V Finkel[2], Claire E Widdicombe[3], Andrew J Irwin[1]

[1] Mathematics & Computer Science, Mount Allison University, Sackville, NB, Canada, E4L 1E6

[2] Environmental Science, Mount Allison University, Sackville, NB, Canada, E4L 1A7

[3] Plymouth Marine Laboratory, Prospect Place, Plymouth, UK, PL1 3DH

Keywords: Phytoplankton, time-series, traits, growth rate, grazing rate, English Channel

Abstract

Phytoplankton trait-based modeling is a mechanistic approach to describing species and community dynamics in ecosystem models. Trait values are usually extracted from laboratory studies of single species, which presents challenges for understanding the immense diversity of phytoplankton species and the wide range of dynamic ocean environments. Here we use a Bayesian approach and a trait-based model to extract traits for four functional types and ten diatom species from field data collected at Station L4 in the Western Channel Observatory. We find differences in maximum net growth rate, temperature optimum and sensitivity, half-saturation constants for light and nitrogen, and density-dependent loss terms across the functional types. We find evidence of very high linear loss rates, suggesting that grazing may be even more important than commonly assumed and differences in density-dependent loss rates across functional types, indicating the presence of strong niche differentiation among functional types. Very low half-saturation constants for nitrogen at the functional type level may indicate widespread mixotrophy. At the species level, we find a wide range of density-dependent effects, which may be a signal of diversity in grazing susceptibility or biotic interactions. This approach may be a way to obtain more realistic and better-constrained trait-values for functional types to be used in ecosystem modeling.

Introduction

Phytoplankton perform about half of global photosynthesis, form the base of the marine food web and are an important driver of biogeochemical cycles (Field et al. 1998). Model projections of changes in phytoplankton primary production with climate over the next century are extremely variable (Finkel et al. 2010, Finkel 2014). Projections of changes in communities and biogeochemical cycling usually depend on mechanistic models of phytoplankton productivity parameterized with traits of phytoplankton species (Le Quéré et al. 2005, Litchman et al. 2006). The traits used in models vary according to the research questions, but most commonly include maximum growth rate, Arrhenius-like temperature effects on growth rate, half-saturation parameters linking the growth rate to resource availability, and grazing susceptibility (Litchman et al. 2007, Irwin & Finkel 2016). At present, many of these parameters are not well constrained for phytoplankton communities (Anderson 2005, Irwin & Finkel 2016).

Phytoplankton are evolutionarily and ecologically diverse and include many phyla and tens of thousands of species (Sournia et al. 1991, de Vargas et al. 2015). This complexity presents several challenges for trait-based modeling. Trait values measured in the lab are almost always determined for a few key species, while their application in models of natural communities usually apply to dozens to thousands of species. The aggregation of similar species into biogeochemically defined functional types greatly simplifies models, but there is no clear way to decide which species should be used as representatives of each functional type (Merico et al. 2004, Le Quéré et al. 2005, Hood et al. 2006). Trait values for species in the same functional type and trait values used in models vary widely, commonly by a factor of 10-100 (Anderson 2005, Irwin & Finkel 2016). It is not clear how to average trait values across species to represent a functional type since phytoplankton growth rate is a non-linear function of trait values. Furthermore, species well adapted to lab conditions may not be representative of their respective functional types growing in natural communities. A second set of challenges concerns the difficulty of using lab-based estimates of trait values in a field context. Trait values quantified using laboratory cultures under controlled conditions are stable under repeated measurement, but there is a challenge in identifying the most appropriate conditions for culture experiments. For example, the maximum growth rate is commonly estimated in the lab, but

differences in culture conditions from one lab to another means there is always some doubt about the true maximum growth rate for a species (Boyd et al. 2013). Trait-values, including maximum growth rate and nutrient uptake rates, estimated in the field can differ substantially from those measured in the lab (Furnas 1991, Laws 2013, Lomas et al. 2014). Cultures grown under equilibrium conditions in the lab may not reveal key acclimation traits or the consequences of environmental variability that can be crucial to the fate of phytoplankton in natural communities (Grover 1991, Raven 2011). In summary, trait values for most phytoplankton species are not available and we do not currently have enough data to strongly constrain trait values used in functional type models (Anderson 2005, Flynn et al. 2015).

An approach that addresses many of these challenges for determining trait values for function types is to estimate those values from long-term time series of natural communities observed in the field. Our goal is to obtain quantitative estimates of trait values that define the dynamics of the biomass of phytoplankton functional types. These trait values will be affected by the species that are present in the community, the range of environmental conditions observed, the spectrum of environmental variability, as well as abiotic and biotic interactions, so we call them realized traits in recognition that they are not the fixed traits of a particular species. This label is an echo of the difference between fundamental and realized niches, where the realized niche is measured in a community and can differ from the fundamental niche (Hutchinson 1957, Colwell & Rangel 2009). Here we obtain realized trait values by fitting a model of biomass dynamics to time series of phytoplankton functional type biomass and coincident environmental conditions. The model describes temporal biomass changes in terms of net growth rate modified by temperature, irradiance, total available nitrogen concentration, and a density dependent loss term. We adopt a hierarchical Bayesian modeling approach and use Markov-chain Monte Carlo (MCMC) methods to simulate from the joint posterior of the model parameters, in particular the traits of interest. Realized trait values estimated from field data may be quite different from trait values obtained in the lab and may vary across communities in different locations. The advantages of these realized traits compared to species-level traits quantified in the lab is that these traits by definition describe observed community dynamics.

Methods

Data

We used data from the Western Channel Observatory (WCO) oceanographic time-series (www.westernchannelobservatory.org.uk) in the Western English Channel. The WCO data include phytoplankton, zooplankton, and fish trawls together with measurements of several physical and chemical environmental parameters such as temperature, salinity and nutrient concentrations. The data used here were collected at Station L4 (50° 15.00′N, 4° 13.02′W) located about 10 km south of the Plymouth breakwater with a water column depth of about 50 m (Harris 2010). We used 349 weekly observations of taxonomically resolved phytoplankton abundance, temperature, nitrate, nitrite, and ammonium concentrations sampled at 10 m depth in the upper mixed layer and sea-surface irradiance collected over a 7-year period spanning 15 April 2003 through 31 December 2009. Average biovolume measurements were recorded for each species (Widdicombe et al. 2010) and converted to carbon content (Menden-Deuer & Lessard 2000) to obtain biomass concentrations (mg C m^{-3}) for each species. We used observations of 193 taxonomic categories identified as 138 species, 27 genera, and 28 size-classes for broader morphological categories. Biomass concentrations were aggregated into four functional types: diatoms, dinoflagellates, coccolithophorids, and phytoflagellates. The phytoflagellate type is taxonomically diverse but is dominated (more than 50% of the biomass) by unidentified flagellates less than 5 μm in diameter. Some species may be benthic or tychoplanktonic. We added together the concentrations of nitrate, nitrite, and ammonium to obtain a single inorganic nitrogen (mg m^{-3}) concentration. Most of the variation in total nitrogen concentration is due to variation in nitrate concentration. Irradiance (mol m^{-2} d^{-1}) was measured continuously above the sea-surface near Station L4 at Plymouth and averaged over the day. Data for missing weeks were imputed by linear interpolation using the na.approx function from the zoo library in R (R Core Team 2016).

The model

We describe the multiplicative growth rate of each functional type's biomass as the product of the following 5 components: (i) a net growth rate reduced by limitation due to

either low light or low nitrogen concentration, (ii) a temperature effect, (iii) a density feedback term dependent on the biomass of the focal functional type, (iv) a density feedback term dependent on the biomass of all phytoplankton not in the focal functional type, and (v) a positive multiplicative noise term. The change in biomass from one week to the next (from week *w*–1 to week *w*) for each functional type i is modeled by multiplying the biomass in week *w*–1 by the (multiplicative) growth rate according to a stochastic Gompertz model (Saitoh et al. 1997, Mutshinda et al. 2009, Mutshinda et al. 2011). We chose to model the net growth rate as a linear combination of density-independent growth rate and density-dependent losses, which is most appropriate given the lack of direct information about grazing rates, grazer biomass, or viral abundance. Therefore, the biomass concentration $Y_{i,w}$ (in $\mathrm{mg\,C\,m^{-3}}$) of the ith functional type for each week after the first $(w \geq 2)$ is described by

$$Y_{i,w} = Y_{i,w-1} \exp\left\{ r_{i,w} + \alpha_i \log(Y_{i,w-1}) + \phi_i \log(Z_{i,w-1}) \right\} \eta_{i,w}\,, \qquad (1)$$

where $Z_{i,w}$ is the combined biomass concentration of all phytoplankton not including the ith functional type during week *w*. The growth rate, which appears in the exponent of Eq. (1), is composed of a density-independent component, $r_{i,w}$, and a density-dependent component, $\alpha_i \log(Y_{i,w-1}) + \phi_i \log(Z_{i,w-1})$. Stochastic noise enters the biomass dynamical model (Eq. 1) through the random multiplicative noise $\eta_{i,w} > 0$ that we assume to be serially independent and log-normally distributed with median one and mean $\exp(\sigma_{i,w}^2/2)$, so that the $\log(\eta_{i,w})$ are independently zero-mean normal with respective variances $\sigma_{i,w}^2$. The unstructured stochastic noise term lumps together the variability due to all un-modelled processes: demographic stochasticity, sampling error and the environmental variability attributable to other variables not included in the model. The log-normal distribution is widely used to describe species abundance and biomass patterns (MacArthur 1960, Sugihara 1980) on both theoretical and empirical grounds. We showed that biomass

distributions at this site are log-normal in an earlier study (Mutshinda et al. 2016). The notation is summarized in Table 1.

The traits to be estimated appear in the growth rate terms. The density-independent component of growth rate, $r_{i,w}$, for functional type i from week w-1 to week w depends on Michaelis-Menten functions of irradiance (PAR, mol m^{-2} d^{-1}) and nitrogen concentration (N, μmol L^{-1}), and a function of temperature (T, °C), according to

$$r_{i,w} = \mu_i \min\left(\frac{PAR_{w-1}}{k_{E,i}+PAR_{w-1}}, \frac{N_{w-1}}{k_{N,i}+N_{w-1}}\right) - \beta_i |T_{w-1} - \theta_i| \quad (2)$$

where θ_i denotes the optimum growth temperature for the biomass of functional type i and $\beta_i > 0$ is a temperature sensitivity parameter intended to quantify the increase in the density-independent growth rate $r_{i,w}$ for a 1°C change in temperature towards the optimum temperature θ_i and *vice-versa*. The optimal temperatures θ_i for growth of each functional type are assigned priors and estimated from the data within our Bayesian framework. Saturating functions of irradiance and nitrogen concentration and their combination with a minimum function are commonly used to moderate growth rate (Denman & Peña 1999, Healey et al. 2009). The net growth rate $\mu_i > 0$ is the density-independent growth rate of the ith functional type at optimal temperature, irradiance and nitrogen concentration. The effects of irradiance and nitrogen concentration on the growth rate are represented by saturating functions parameterized by the half-saturation constants $k_{E,i} > 0$ and $k_{N,i} > 0$ which are respectively the irradiance level and nitrogen concentration at which the net growth rate at optimal temperature drops to $\mu_i / 2$. The Michaelis-Menten saturating functions are combined with a minimum function so that only the most limiting resource affects growth rate at a time, according to Liebig's law of the minimum (van der Ploeg & Kirkham 1999). During model development, we explored the possibility of a multiplicative interaction between light and nutrients, but found the results to be more difficult to interpret.

To accommodate density-dependent factors including grazing, viral attack, aggregation and sinking, we introduce density dependent loss terms. In the absence of direct observations of these losses, we parameterize the density-dependent losses with α_i

and ϕ_i to quantify the feedbacks on the growth rate of the ith functional type from its own biomass and from the combined biomass of the other functional types in the community, respectively. The terms involving α_i and ϕ_i distinguish two different density-dependent loss terms, which could result from specialist and generalist grazer populations. For the purposes of estimating the parameters in the model, we rewrote Eq. (1) on the natural logarithmic scale as

$$y_w = y_{w-1} + \mu_i \min\left(\frac{PAR_{w-1}}{k_{E,i}+PAR_{w-1}}, \frac{N_{w-1}}{k_{N,i}+N_{w-1}}\right) - \beta_i|T_{w-1} - \theta_i| + \alpha_i y_{i,w-1} + \phi_i z_{i,w-1} + \varepsilon_{i,w} \quad (3)$$

where $y_{i,w} = \log(Y_{i,w})$, $z_{i,w} = \log(Z_{i,w})$ and $\varepsilon_{i,w} = \log(\eta_{i,w}) \sim N(0, \sigma^2_{i,w})$.

We adapted the functional-type level model described above to define traits at the species level. This task was challenging for two reasons: the greatly increased number of parameters to be estimated and the fact that most species are absent from the time series for most of the time, either because they were absent or their abundance was below the detection limit. By contrast, missing values were rare in the time series of functional type biomasses. We restricted the species-level analysis to the 10 diatoms that were observed in about half of the sampling occasions or more. These species may not be representative of the functional type dynamics as a whole because the selected species only represent 11% of the diatom functional type biomass. In order to estimate a growth rate, biomass observations for any particular species must be available on numerous pairs of successive weeks. We extracted pairs of observations from the full time series to estimate the growth rate from week *w-1* to *w*, conditioned on the species being observed during week *w-1*. The species-level model differed from Eqns. (1-3) only in the definition of the biomass terms $Y_{i,w}$ and $Z_{i,w}$ and the interpretation of the density-dependent terms α and ϕ. To emphasize the differences between the functional type and species-level models, we have added a superscript *S* to the notation for each trait in the species-level model. In the species model, $Y_{i,w}$ was the biomass of species i in week *w*, and $Z_{i,w}$ was the sum of the biomass of all species in the same functional type as species i except for species *i* in week *w*. The density-dependent parameter α reflected the effect of species *i* on itself while ϕ described the

density-dependent loss due to all species in the same functional type as species *i* except for species *i*.

The model was developed and fit to the data with a Bayesian approach (Gelman et al. 2013). Bayesian inference is an approach to statistical inference where all unknown quantities are considered as random variables. The uncertainty about plausible values of an unknown quantity θ before the data is taken into consideration is represented by a probability distribution $p(\theta)$ called the prior distribution. Upon observing the data, the prior distribution is combined with the likelihood function (the sampling distribution of the data) $p(y \mid \theta)$ through Bayes' rule to produce a posterior distribution $p(\theta \mid y)$

$$p(\theta \mid y) = \frac{p(y \mid \theta) p(\theta)}{p(y)}, \tag{4}$$

where $p(y) = \int_{\Theta} p(y \mid \theta) p(\theta) d\theta$ is the marginal distribution of the data which is the normalizing constant making $p(\theta \mid y)$ a proper probability distribution. Therefore, Eq. (4) can be written as

$$p(\theta \mid y) \propto p(y \mid \theta) p(\theta). \tag{5}$$

where $\propto$ stands for " proportional to".

The posterior distribution represents the data-updated knowledge and forms the basis of Bayesian inference about unknown quantities including model parameters, missing values, and yet unseen data. Having an entire distribution rather than point estimates allows one to fully account for uncertainty. Bayesian conclusions are essentially probability statements based on the posterior distribution. All Bayesian computations are based on probability rules, resulting in more intuitive statements than counterparts in classical statistics.

The hierarchical priors in the Bayesian model allowed us to specify a model with many traits for many functional types or taxonomic units without risking over-fitting the data or running into convergence problems that plague other nonlinear optimization methods. The shared hyper-priors effectively pooled data across taxa when there are few data while allowing trait value estimates to be differentiated across taxa when supported by the data. The model fitting to the functional type biomass data was based on the following essentially non-informative prior distributions for the model parameters.

$k_{E,i} \sim \mathrm{N}(0,100)\,\mathrm{I}(k_{E,i} > 0)$, where $\mathrm{I}(.)$ denotes the indicator function which takes the value 1 when its argument is true and the value 0 otherwise, $k_{N,i} \sim \mathrm{N}(0,10)\,\mathrm{I}(k_{N,i} > 0)$, $\beta_i \sim \mathrm{N}(0,1)\,\mathrm{I}(\beta_i > 0)$, $\theta_i \sim \mathrm{N}(\overline{T},10)$, where $\overline{T}$ is the mean temperature over the study period, $\alpha_i \sim \mathrm{N}(0,1)$, $\phi_i \sim \mathrm{N}(0,1)$, $\sigma^2_{i,w} \sim \mathrm{InvGamma}(a,b)$, $a \sim \mathrm{Gamma}(1,1)$ and $b \sim \mathrm{Gamma}(1,1)$. We imposed fairly informative $\mathrm{Gamma}\,(5,5)$ priors independently on the net growth rates μ_i to enforce identifiability. For the species model, the hierarchical priors were designed to provide identical trait estimates for all species if the data did not oppose this possibility.

The main problem of Bayesian inference comes from the difficulty in evaluating integrals like the one in the denominator of Eq. (4). In most practical cases the posterior is not available in closed form so sampling-based algorithms, mostly Markov chain Monte Carlo (MCMC) methods (Gilks 1996) are used to simulate from it and base inferences on the simulated sample. Markov chain Monte Carlo methods indirectly simulate from a distribution g when direct simulation from g is difficult or impossible. The rationale of MCMC sampling is to set up a Markov chain whose stationary distribution is the distribution g of interest, in this case the joint posterior distribution $p(\theta \mid y)$. Consequently, simulation of $\theta^{(1)}, \theta^{(2)}, \ldots$ from the chain yields a series with the property that the marginal density of $\theta^{(j)}$ for large enough j is approximately g. In other words, for a large enough "burn-in" period n, $\theta^{(n+1)}, \theta^{(n+2)}, \ldots$ can be regarded as a dependent series with marginal density g. Therefore, empirical moments of this series yield approximations of the moments of g.

We used Markov chain Monte Carlo (MCMC) simulation (Gilks 2005) implemented in OpenBUGS (Thomas et al. 2006) to sample from the joint posterior of the model parameters. We assessed the convergence of the Markov chains through visual inspection of traceplots and autocorrelation functions. We ran three parallel Markov chains starting from dispersed initial values for 60,000 iterations and discarded the first 30,000 samples from each Markov chain as burn-in. We used the remaining 30,000 samples to generate the posterior distributions on our parameters, retaining every 30th sample to reduce the sample autocorrelation. Our results were robust to changes in the range of priors.

Results

The three environmental drivers of phytoplankton growth rate included in this study (temperature, irradiance, and nitrogen concentration) exhibit strong, regular seasonal oscillations over the seven-year time series (Widdicombe et al. 2010, Mutshinda et al. 2016). The phytoplankton biomass for each of four functional types each exhibit distinctive patterns of intra-annual variation (Fig. 1). Diatoms bloom first, increasing steadily in biomass from day 60 to day 180. Dinoflagellates and coccolithophorids bloom slightly later, reaching a maximum biomass at approximately day 225. The amplitude of dinoflagellate biomass is the greatest across the four types and their sustained maximum growth and loss rates are also the largest. Phytoflagellates have the least inter-annual variability, with two minor biomass peaks at approximately day 110 and day 215. Our model is able to describe the biomass dynamics, explaining on average between 51% (for diatoms) and 95% (for phytoflagellates) of the variation in the biomass of individual functional types. More importantly, the model produces accurate biomass predictions reflected in narrow, relative to the total variation in the data, posterior predictive intervals (Fig 1). There was insufficient temporal resolution in the data to observe short-term acclimation to changing conditions, so our focus remained on steady-state traits similar to those usually used in phytoplankton community models.

Functional-type level analysis

The maximum net growth rate trait, μ_i, is the largest growth rate of functional type i under any irradiance and nutrient conditions, at its optimal temperature for growth, not including density-dependent grazing, but incorporating linear grazing rates. There is substantial variability in the maximum net growth rate between functional types (whiskers on Fig. 2a). As a group, diatoms have the largest net growth rate with median doubling time 3.9 days, followed by dinoflagellate with mean doubling time 5.5 days, and phytoflagellate with mean 6.7 days. Coccolithophores have the lowest net growth rate with median doubling time 8.9 days.

The estimated optimal temperatures for growth for diatom, dinoflagellate, coccolithophorid, and phytoflagellate biomass are 15°C, 20°C, 19°C and 11°C, respectively, implying that higher temperature conditions would favor dinoflagellate and coccolithophorid biomass accumulation (Fig. 2b). As a group, dinoflagellates are the most responsive to temperature changes with a sensitivity parameter roughly twice as large as those of diatoms and coccolithophorids (Fig. 2c). On the other hand, the phytoflagellate biomass is essentially insensitive to temperature changes at Station L4.

The nitrogen (nitrate, nitrite, plus ammonia) half-saturation constants, k_N, for all groups are comparable to those found in lab studies and used in models (Fig. 2d). The phytoflagellates have the smallest half-saturation constants for irradiance, which is consistent with their relatively small amplitude of biomass variation over the time series. The half-saturation constants for irradiance are not credibly different from one another for the other three phytoplankton functional types and exhibit variability of two-fold or more within their 95% credible intervals (Fig. 2e). The half-saturation constants for nitrogen concentration (posterior means ranging from 0.02-0.3 μmol L^{-1}) are quite close to the minimum values of the corresponding environmental data observed over the time-series (0-15 μmol L^{-1}), which suggests that this trait may not be particularly informative for predicting the growth rate of these functional types at this location for most of the year. Conversely, the half-saturating constants for sea-surface irradiance (10-30 mol m^{-2} d^{-1}) span most of the lower half of the inter-annual variation in irradiance (10-50 mol m^{-2} d^{-1}), indicating that phytoplankton growth rates vary with irradiance (light is sub-saturating) for much of the year (Fig. 2e).

All four phytoplankton functional types are affected by density-dependent loss rates (Fig. 2f). These losses have the largest effect at high biomass concentrations and can explain the maximum biomass concentration for each functional type, but they are also active at low biomass concentrations and these loss terms are responsible for decreases in biomass when growth conditions are unfavorable. Density-dependent losses are a combination of grazing, viral attack, and aggregation and sinking following bloom collapse. For each functional type, we distinguished between density-dependent feedback due to the functional type's own biomass (α) and the feedback due to the aggregate biomass of all the other functional types (ϕ). If the density-dependent loss terms are primarily due to grazing,

we could interpret α as representing losses due to grazers specializing on one functional type and ϕ as representing losses due to generalist grazers supported by populations of the other functional types. Since $\alpha < 0$ for all functional types, but ϕ is not different from 0 for all types, the biomass of each functional type is largely regulated by specialist grazers and generalist grazers have weak density-dependent effects.

Species-level analysis

Diatom species' net growth rates were smaller than the functional type counterpart for all ten species examined (Fig. 3a). At the functional-type level, diatoms were weakly affected by temperature ($\beta < 0.1$ week^{-1} °C^{-1}) and this result carried through for the diatom species (most β^S close to 0.1, Fig. 3b). The optimal temperatures were extrapolated outside the range of observed temperatures, and thus are very uncertain (data not shown). Diatom species' half-saturation constants for irradiance are lower than the functional type counterpart whereas diatom species' nitrogen half-saturation constants are higher than the functional type level estimate.

For the species model, the density dependent loss analysis was redesigned to identify species-specific density-dependent loss rates and generic functional type density-dependent loss rates. The posterior distributions of the species-level density dependent parameters α^S and ϕ^S imply a stronger negative feedback on each diatom species' biomass growth from its own biomass than that from the combined biomass of other diatom species i.e., $\alpha^s < \phi^s$ (Fig. 3e)^S), consistent with niche differentiation within functional types (Mutshinda & O'Hara 2011). Some of the α^S and ϕ^S for diatoms were positive, suggesting the presence of mutually beneficial or commensal effects in some species.

Discussion

Trait-based models of phytoplankton productivity promise to deliver robust projections of phytoplankton community dynamics under future climate scenarios. Phytoplankton traits are estimated in the lab one species at a time but are commonly aggregated into functional types for ocean biogeochemical models (Anderson 2005, Le Quéré et al. 2005, Litchman et al. 2006). There are several challenges that arise in the

357 estimates of phytoplankton traits for trait-based models. Most species in diverse
358 communities have not been systematically studied in the lab. Trait values vary across
359 species, even within functional types, and it is not clear how to produce an average trait
360 value for modeling functional types. In addition, there is considerable phenotypic plasticity
361 in traits. Furthermore, grazing rates, viral and parasitic loss rates, sinking rates and biotic
362 interactions, such as allelopathy or mutualisms, can be complex and highly variable from
363 species to species. It is difficult to get good estimates of loss terms, such as grazing rate and
364 viral lysis, that are inherently species specific and patchy in time and space, and we are just
365 starting to learn about the consequences of the many, complex biotic interactions between
366 phytoplankton and their microbial communities (Sher et al. 2011, Amin et al. 2015). It may
367 be possible to overcome some of these myriad challenges using phytoplankton traits
368 estimated directly from field data or by combining lab-based traits with niches estimated
369 from the field (Edwards 2016). Here we extract functional-type and species-level
370 phytoplankton traits from time-series data from a well-studied coastal temperate
371 phytoplankton community in the Western English Channel (Harris 2010, Widdicombe et al.
372 2010). While some of the traits estimated here are consistent with laboratory estimates of
373 similar traits on single species in the lab, many are not, indicating more work is needed to
374 understand how phytoplankton respond in natural communities.
375 Our estimates of maximum net growth rate for the phytoplankton functional types
376 range from 0.4 to 1.5 week^{-1} (a doubling time of 3.2 to 12 days) and for 10 individual
377 diatom species from 0.99 to 1.57 week^{-1} (a doubling time of 6.9 to 11 days). Our growth
378 rate estimates are considerably lower than lab-based estimates of growth rate from
379 unialgal cultures and *in situ* field estimates of growth rate of individual species (grazers
380 excluded) that can double more than once a day (Furnas 1990, 1991, Raven et al. 2005).
381 Maximum *in situ* growth rates for three of our ten diatom species have been estimated from
382 daily counts during April in the Irish Sea: *Pseudo-nitzchia* sp., 0.24 d^{-1}; *Guinardia delicatula*,
383 0.18 d^{-1}; *Lauderia annulata* 1.42 d^{-1}. These rates range from approximately the same to up
384 to 25 times our estimated maximum net growth rates (McKinney et al. 1997). Weekly
385 counts, used in our study, are likely to lead to smaller maximum net growth rates than daily
386 counts because the coupling between growth and loss processes will be tighter when
387 averaged over a week instead of a day. We expect our estimate of maximum growth rate to

be lower than traditional estimates of individual species growth rates in the lab and field because our growth rate estimates include linear loss terms due to grazing, viral and parasitic loss and are therefore similar to a net phytoplankton community growth rate. Our values for net growth rate are consistent with satellite-based estimates of monthly median phytoplankton growth rates in temperate regions with strong seasonal blooms, 0.35 to 4.2 week^{-1} (Westberry et al. 2008). Microzooplankton grazing at Station L4 and elsewhere has been estimated to account for about two-thirds of phytoplankton growth (Fileman et al. 2002, Calbet & Landry 2004, Chen et al. 2009, Bernard et al. 2012). Given our estimates of maximum growth rates tend to be more than an order of magnitude lower than estimates of growth rate from lab studies, this suggests loss rates due to grazing and parasitoid and viral attack may be higher than often assumed.

It would be plausible for there to be no relationship between our field based estimates of maximum growth rates across the functional types even if there are differences in maximum net growth rate since the grazing and other linear loss terms represent such a large fraction of maximum net growth rate. We find the rank order in our estimates of net growth rates for the functional types (diatoms > dinoflagellates > phytoflagellates > coccolithophorids) are generally consistent with growth rates reported from laboratory culture work and field observations (Furnas 1991, Cermeño et al. 2005, Raven et al. 2005, Laws 2013). In the Western English Channel we find diatoms have the largest maximum net growth rate, which is roughly double that of coccolithophorids and phytoflagellates (Fig. 2a). These results indicate that lab-based maximum growth rates combined with a constant loss rate used by many models may be a reasonable proxy for net growth rates in natural communities.

The effect of temperature on phytoplankton species growth rates is commonly described using the Q_{10} approximation, which is the multiplicative effect of a 10°C change in temperature on growth rate. This value is typically about 2, ranging from 1.88 to 2.3 for phytoplankton (Eppley 1972, Bissinger et al. 2008). The range of temperatures at Station L4 (about 8-18°C) is narrow compared to the width of many phytoplankton temperature niches (Irwin et al. 2012, Boyd et al. 2013) so we used a linear model to describe the effect of temperature on growth rate (see Montagnes et al. 2003 for additional rationale for using a linear model). The temperature sensitivity of the functional types, β, is about 0.11 week^{-1}

419 °C^{-1} for dinoflagellates, 0.06 week^{-1} °C^{-1} for coccolithophorids and 0.05 week^{-1} °C^{-1} for
420 diatoms, meaning that growth rate would increase from roughly 1 week^{-1} to 1.7 week^{-1} for
421 dinoflagellates, from 1 week^{-1} to 1.4 week^{-1} for coccolithophorids, and from 1 week^{-1} to 1.3
422 week^{-1} for diatoms with an increase in temperature of 6°C (half the annual amplitude in
423 temperature) starting below their temperature optimum (Fig. 2c). Analysis of the change in
424 maximum growth rate with temperature from unialgal lab cultures (Montagnes et al. 2003)
425 found a slope 0.11 to 0.54 week^{-1} °C^{-1} for dinoflagellates, which is comparable to the
426 posterior means (0.11 week^{-1} °C^{-1}) found in this study (Fig. 2c), and 0.084 to 0.97 week^{-1} °C^{-}
427 ^{1} for diatoms which is higher than the posterior mean (0.055 week^{-1} °C^{-1}) found in this
428 study. For phytoflagellates our temperature trait β is 0.017 week^{-1} °C^{-1} which is close to
429 zero and the credible interval is narrow and close to 0, so we conclude that temperature
430 has essentially no effect on the growth rate of this functional type at this site. Possible
431 interpretations for this result are that the phytoflagellates have broad temperature optima
432 for growth rate or the functional type is composed of many species with specialized
433 optimal growth temperatures spread across the range of observed temperatures (Eppley
434 1972, Boyd et al. 2013). This does not appear to be the case for dinoflagellates and
435 coccolithophorids; even if there is species turnover during the year, there is still a strong
436 imprint of temperature on the growth rate of the functional type as a whole. An alternative
437 explanation is that an increase in water column stability favors an increase in dinoflagellate
438 and coccolithophorid biomass accumulation (Margalef 1978, 1997). The optimal
439 temperature for growth at the functional type level varies as expected with diatoms and
440 phytoflagellates having lower optimal temperatures than dinoflagellates and
441 coccolithophorids, which bloom later in the season. Since temperature is correlated with
442 stability and we don't have an independent measure of stability, our model is unable to
443 distinguish between the direct effects of temperature and the effect of water column
444 stability on the growth rate of phytoplankton.
445 Temperature optima for individual diatom species were not identified within the
446 range of observed temperatures (not shown); we interpreted these results as consistent
447 with wide temperature response curves, relative to the narrow temperature range at
448 Station L4, for each species (Boyd et al. 2013). The estimates of the strength of the
449 temperature effect for individual diatom species (β^S, Fig. 3b) was roughly twice as high as

450 the effect on the diatom functional type. Averaging responses over many species in a
451 functional type could lead to weaker effects of temperature change as contrasting effects of
452 temperature on individual species partially cancel each other out.
453 Light and nutrient limitation of net growth rate is determined by Michaelis-Menten
454 half-saturation trait values, k_N and k_E. Three sources of inorganic nitrogen: nitrate, nitrite,
455 and ammonium are considered in our estimate of k_N for inorganic nitrogen. As a result our
456 estimate of k_N at the functional type level is largely determined by the inorganic nitrogen
457 species with the smallest half-saturation constant. Half-saturation constants for nitrogen
458 for phytoplankton species can vary from 0.08 to 8.4 μmol L^{-1} in the lab (Litchman et al.
459 2006). Our half-saturation constants for individual diatom species, many with large cell
460 size, ranged from 1.2-5 μmol L^{-1}, which is comfortably within this range. Our values for
461 functional types range from about 0.02 to 0.22 μmol L^{-1}, and are either on the lower end or
462 smaller than typical literature values for unialgal cultures. Diatoms and dinoflagellates as
463 functional types have k_N approximately a factor of ten smaller than many lab-based
464 literature estimates. The half-saturation constants for inorganic nitrogen for the
465 phytoplankton functional types at the site are also low relative to all but the lowest
466 nitrogen concentrations observed in seawater at this site (ranging from 0.1-16 μmol L^{-1},
467 only 10% of observations are less than 0.20 μmol L^{-1}), indicating that nitrogen limitation is
468 only a significant factor affecting growth rates of functional types, particularly diatoms and
469 dinoflagellates, in the warmest part of the summer. One reason k_N may be lower in the field
470 relative to laboratory studies is that organic nitrogen may be an important source of
471 nitrogen for some species, particularly the dinoflagellates and phytoflagellates, but also
472 some diatoms such as *Pseudo-nitzschia delicatissima* (Loureiro et al. 2009). If organic
473 sources are important for these groups, for example following the crash of a diatom bloom
474 when inorganic nitrogen concentrations are low, estimated k_N may be artificially low since
475 organic sources were not included in the model. Alternatively, since nitrogen is taken up
476 rapidly when available, bulk estimates of reactive nitrogen concentration sampled weekly
477 may be relatively uninformative at physiological scales (Laws 2013). The phytoflagellates
478 have the lowest k_N of approximately 0.02 μmol L^{-1}, which is less than half the value for
479 diatoms and roughly 10% of the value of coccolithophorids (Fig. 2d). The phytoflagellate
480 category is taxonomically diverse, but over half the biomass is found in unidentified cells

smaller than 5 μm in diameter. The resulting high surface area to volume ratio is consistent with very low k_N (Fiksen et al. 2013). The most significant feature of our results is that the phytoplankton dynamics at Station L4 is consistent with very low k_N compared to values estimated from laboratory cultures (Litchman et al. 2007). The k_N at Station L4 are 5-10 fold smaller than half-saturation constants for nitrate often employed in ecosystem models (Gregg et al. 2003, Merico et al. 2004). The intermediate complexity marine ecosystem model constructed by Moore et al (2002) is an exception; this model uses a very low k_N for ammonium of 0.004 μmol L^{-1} for small cells, much lower than our values for Station L4 (Moore et al. 2002). Generally k_N for ammonium are smaller than values for nitrate (Litchman et al. 2007; Merico et al. 2004).

Light limitation is frequently parameterized by a half-saturation coefficient, k_E, or the irradiance at which light saturates growth, E_k. For comparison between the two, we divide E_k by 2 to roughly approximate k_E. In natural populations in coastal regions, E_k varies from 40-500 μmol m^{-2} s^{-1} (Kirk 2010), corresponding to k_E of about 2-22 mol m^{-2} d^{-1}. Estimates of k_E in unialgal cultures range from 3.5-7.8 mol m^{-2} d^{-1} (Litchman et al. 2006), and varies with steady state irradiance (Gregg et al. 2003, Kirk 2010). At Station L4, our values of k_E range from 8 to 20 mol m^{-2} d^{-1}, but these are based on sea-surface irradiance and thus are larger than they would be based on average *in situ* irradiances. Individual diatom species have k_E ranging from 6-14 mol m^{-2} d^{-1}, closer to the values for unialgal cultures. These results suggest that irradiance at Station L4 is limiting for diatoms, dinoflagellates and coccolithophorids during much of the year, since sea-surface PAR ranges from 10-50 mol m^{-2} d^{-1} and only exceeds $E_k \cong 2k_E \cong 40$ mol m^{-2} d^{-1} for these groups during short periods in the summer. By contrast, phytoflagellates have k_E near the minimum levels of PAR and so they experience saturating irradiance for most of the year. One possible hypothesis is that their small size confers a low pigment package effect, meaning they have high light absorption per unit of pigment, giving them an advantage over functional types with larger cells under low light conditions (Finkel & Irwin 2000, Finkel 2001, Finkel et al. 2004). Furthermore, if some of the phytoflagellates use alternative energy sources, they may require less chlorophyll and be less sensitive to changes irradiance. While some dinoflagellates are known to be heterotrophic and mixotrophic (Stoecker 1999), unlike phytoflagellates their growth rate is strongly affected by low

temperatures in winter, reducing their growth rate in winter relative to phytoflagellates (Fig. 1). Phytoflagellates appear to be able to acclimate to very low light, giving them a competitive advantage relative to the other functional types, especially in winter.

Many studies of zooplankton grazing focus on the linear grazing rate (Landry & Hassett 1982, Calbet & Landry 2004, Zheng et al. 2015), which in our model is combined with gross phytoplankton growth rate to obtain the maximum net growth rate trait, μ, which is a constant for each phytoplankton functional type. More complex formulations of zooplankton grazing rates permit diel and seasonal variation in grazing rates and non-linear grazing rates (Tsai et al. 2005) or describe prey switching or selectivity by grazers (Gentleman et al. 2003, Vallina et al. 2014), but we do not consider these mechanisms. Our model incorporates density-dependent loss terms to describe consumption of phytoplankton by grazers along with other loss processes. All four functional types exhibit strong density-dependent loss. Assuming the loss term is primarily attributable to grazing, diatoms and phytoflagellates are primarily grazed by specialists ($\alpha < 0$, Fig. 2) and unaffected by generalist grazers ($\phi \cong 0$) while dinoflagellates and coccolithophorids were roughly equally affected by specialist generalist grazers ($\phi \cong \alpha$). The difference between specialist and generalist density-dependent losses is evidence of strong niche differentiation for diatoms and phytoflagellates. The results at the species level are more variable. Six of our ten diatom species exhibit positive density-dependent effects ($\phi^S > 0$, Fig. 3c) with increased biomass of all other diatoms, which could be an indication that these species experience less grazing pressure when the biomass of other diatoms is high ("kill the winner") (Vallina et al 2014). Two species, *Guinardia delicatula* and *Pseudo-nitzschia seriata*, have positive density-dependent effects resulting from their own biomass ($\alpha^S > 0$), indicating that increases in their biomass can increase their own growth rates. Many strains of *Pseudo-nitzschia* have been shown to produce the neurotoxin domoic acid (Bates et al. 1998, Fehling et al. 2004), suggesting this positive density-dependence may be a result of allelopathy, although *G. delicatula* does not produce toxins and *Pseudo-nitzschia delicatissima* has $\alpha^S = 0$. Finally, three species have negative density dependence arising from their own biomass ($\alpha^S < 0$). *Nitzschia closterium* is known to produce mucus that may increase its export at high densities, which is consistent with this result (Najdek et al. 2005).

Our analysis of ten diatom species demonstrates the potential and challenges of this approach for determining trait values and modeling dynamics of individual species. These species were the most frequently observed in the population, but account for only 11% of the total biomass, on average. Species with fewer observations are less likely to yield informative estimates of trait values due to a lack of data, but account for the vast majority of the biomass. Since our ten species sample is a minority component of the diatom community and represents species present much of the year in contrast to species present for only a few weeks at a time, there is no reason to expect the trait values of these species to be representative of the functional type as a whole. In fact, we observed systematic differences between trait values for these species and the diatom functional type: maximum growth rate is lower and k_N is higher for the all the species analyzed relative to the functional type. Even if we had a random sample of species with trait values representative of the full distribution, determining functional-type level trait values by averaging over species with different traits and changing contributions to the total population can lead to errors due to Simpson's paradox (Chuang et al. 2009, Williams & Hastings 2011). The uncertainties across the diatom species are large enough to suggest that the trait values may be largely indistinguishable across many species (Fig. 3). An independent analysis showed that diatoms species at Station L4 exhibit neutral dynamics within the diatom functional type most of the time, indicating that predicting biomass dynamics of individual species may be much harder than predicting the dynamics of the aggregated biomass of a functional type (Mutshinda et al. 2016). While it is appealing to estimate trait values for functional types from knowledge of individual species, it may be more prudent to deemphasize species-level detail and use realized traits estimated from biomass dynamics aggregated to the functional-type level.

Conclusions

This study enables a comparative analysis of trait values used in biogeochemical models of phytoplankton communities and the trait values estimated from lab studies on individual phytoplankton. The realized traits we quantified could be different from those estimated in the lab because they are functional-type level aggregates and include factors such as phenotypic plasticity and biotic interactions that may vary across species and

communities. At Station L4 in the Western English Channel, diatoms have the highest maximum net growth rates, low half-saturation constant for nitrogen, a low temperature optimum and low temperature sensitivity, and high specialist density-dependent loss rates. By contrast, the dinoflagellates have intermediate maximum net growth rates, high temperature optima and sensitivity. Coccolithophorids have the lowest maximum net growth rate, high temperature optimum and intermediate temperature sensitivity, high half-saturation constants for nitrogen and light, and like the dinoflagellates show similar rates of specialist and generalist density-dependent losses. The phytoflagellates have low maximum net growth rate, low optimum temperatures and sensitivities, low half-saturation constants, and intermediate levels of specialist density-dependent losses. The relative differences in maximum net growth rate, specifically the relatively high rates for diatoms, are consistent with differences estimated in the lab and the field, but the absolute magnitude of the rates are considerably lower because our maximum growth rates include linear loss terms. A comparison of our results with traits estimated in the lab and used in models yields a few insights. Grazing and other linear loss rates, as reflected in a reduction of the gross growth rate, appear be even more important than usually appreciated. We see evidence of complex biotic interactions that are difficult to assess in the lab: diatoms and phytoflagellates are more susceptible to specialist loss rates, perhaps indicating specialist grazers or viruses. At the species level, there appears to be evidence of species interactions increasing the net growth rate of individual diatom species. The half-saturation constants for nitrogen are considerably lower than typical lab estimates, consistent with the use of a wide range of reactive nitrogen sources and widespread mixotrophy. There is considerable variation in our estimates of the trait values within phytoplankton functional types, which could be due to real physiological changes arising from acclimation to environmental conditions over time, variation across species within a functional type, or a consequence of insufficient data. Time-series of field data combined with our analysis gives us insight into the mechanisms affecting the dynamics of species and whole functional types in natural populations that may improve our ability to scale-up results from species-level studies in the lab to community dynamics in the ocean.

Acknowledgements

Station L4 phytoplankton biomass and environmental data were provided by the Western Channel Observatory which was funded as part of the UK Natural Environmental Research Council's National Capability. EMS Woodward and C Harris provided the nutrient data. We thank A Atkinson and T Smyth for assistance and advice. ZVF was supported by the National Science and Engineering Research Council (NSERC) of Canada and the Canada Research Chairs program. AJI was supported by NSERC.

Figure 1.

Observed (black line) and predicted (shaded region) $\log_{10}$ carbon biomass (mg C m^{-3}) of each functional type (diatoms, dinoflagellates, coccolithophorids, and phytoflagellates) at Station L4. The prediction region is the 95% credible range of biomass from the functional type model.

Figure 1.

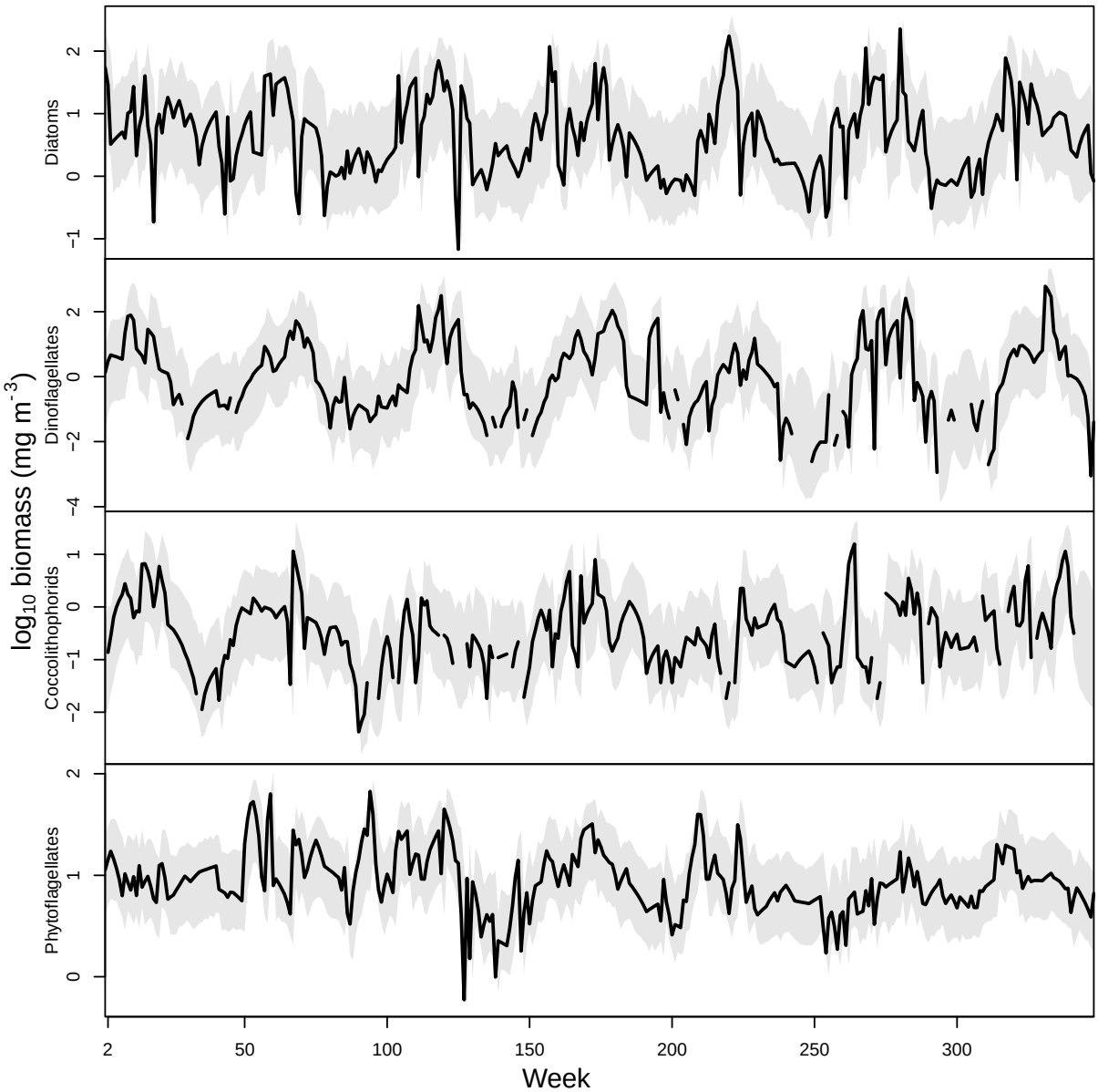
Diatoms
Dinoflagellates
Coccolithophorids
Phytoflagellates
log10 biomass (mg m-3)
Week
2
50
100
150
200
250
300

Figure 2.

Posterior distributions of traits governing growth rate at the functional type level. (a) Maximum net growth rate, μ (week^{-1}), (b) the optimal temperature θ (°C), (c) temperature sensitivity, β (week^{-1} °C^{-1}), (d) the half-saturation constants for nitrogen, k_N (μmol L^{-1}), (e) the half-saturation constants for irradiance, k_E (mol m^{-2} d^{-1}), and (f) density-dependent effects on the growth rate of each functional type attributed to their own biomass (α, solid circle) and to the total biomass of the other functional types in the community (ϕ, open circle). Box plots show median (thick line), the interquartile range (box) and the full range of the data or 1.5 times the interquartile range, whichever is smaller (whiskers). In panels (c) and (f) error bars indicate 95% credible intervals on the posterior means and are used because posterior distribution are approximately normal. In (f), the horizontal dashed line indicates no density-dependence. The vertical scale in (d) is logarithmic to facilitate the display of the wide range of values.

Figure 2.

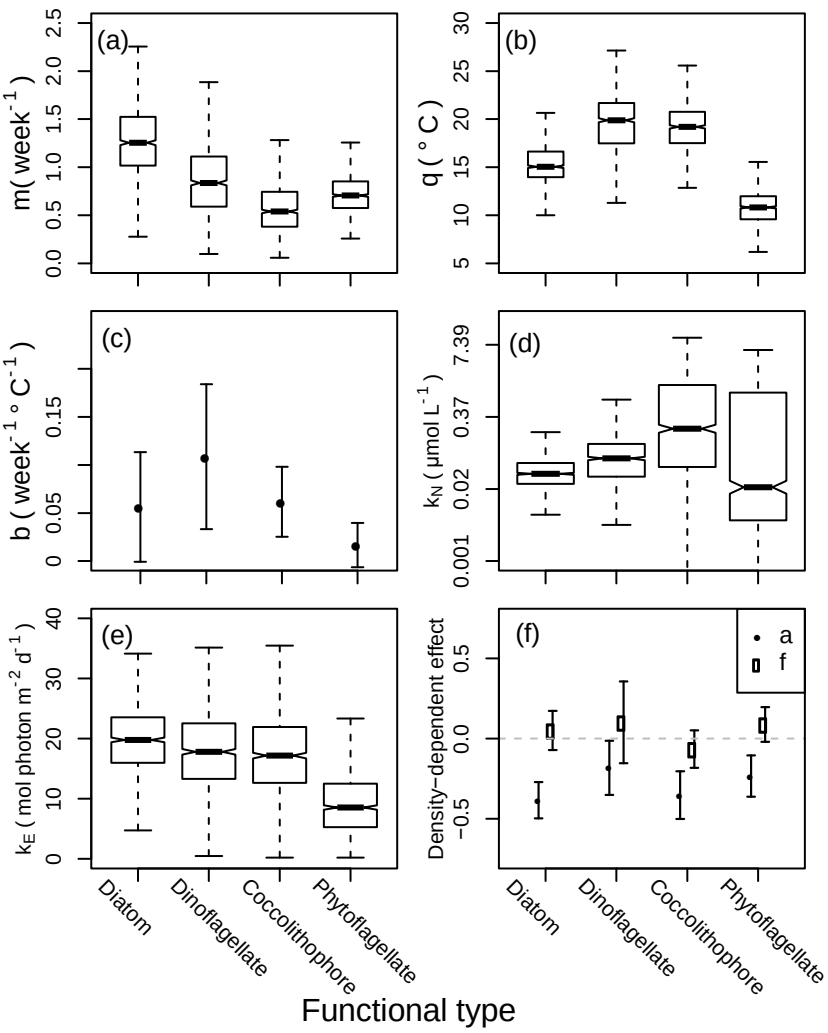
(a)
m(week^{-1})
0.0
0.5
1.0
1.5
2.0
2.5
(b)
q (° C)
5
10
15
20
25
30
(c)
b (week^{-1} ° C^{-1})
0
0.05
0.15
(d)
k_N (µmol L^{-1})
0.001
0.02
0.37
7.39
(e)
k_E (mol photon m^{-2} d^{-1})
0
10
20
30
40
(f)
Density−dependent effect
−0.5
0.0
0.5
a
f
Diatom
Dinoflagellate
Coccolithophore
Phytoflagellate
Functional type

Figure 3.

Species-level trait values for ten diatom species. Species are arranged in order of the number of weeks they are present in the time-series from *Nitzschia closterium* (93% of weeks) to *Lauderia annulata* (48%). (a) Maximum net growth rate, μ^S (week^{-1}), (b) temperature sensitivity, β^S (week^{-1} °C^{-1}), (c) the half-saturation constants for nitrogen, $k_N{}^S$ (μmol L^{-1}), (d) the half-saturation constants for irradiance, $k_E{}^S$ (mol m^{-2} d^{-1}), and (e) density-dependent effects on the growth rate of each functional type attributed to their own biomass (α^S, solid circle) and to the total biomass of the other functional types in the community (ϕ^S, open circle). Box plots show median (thick line), the interquartile range (box) and the full range of the data or 1.5 times the interquartile range, whichever is smaller (whiskers). In panels (b) and (e) error bars indicate 95% credible intervals on the posterior means and are used because posterior distribution are approximately normal. In (e), the horizontal dashed line indicates no density-dependence. The vertical scale in (c) is logarithmic to facilitate the display of the wide range of values.

Figure 3.

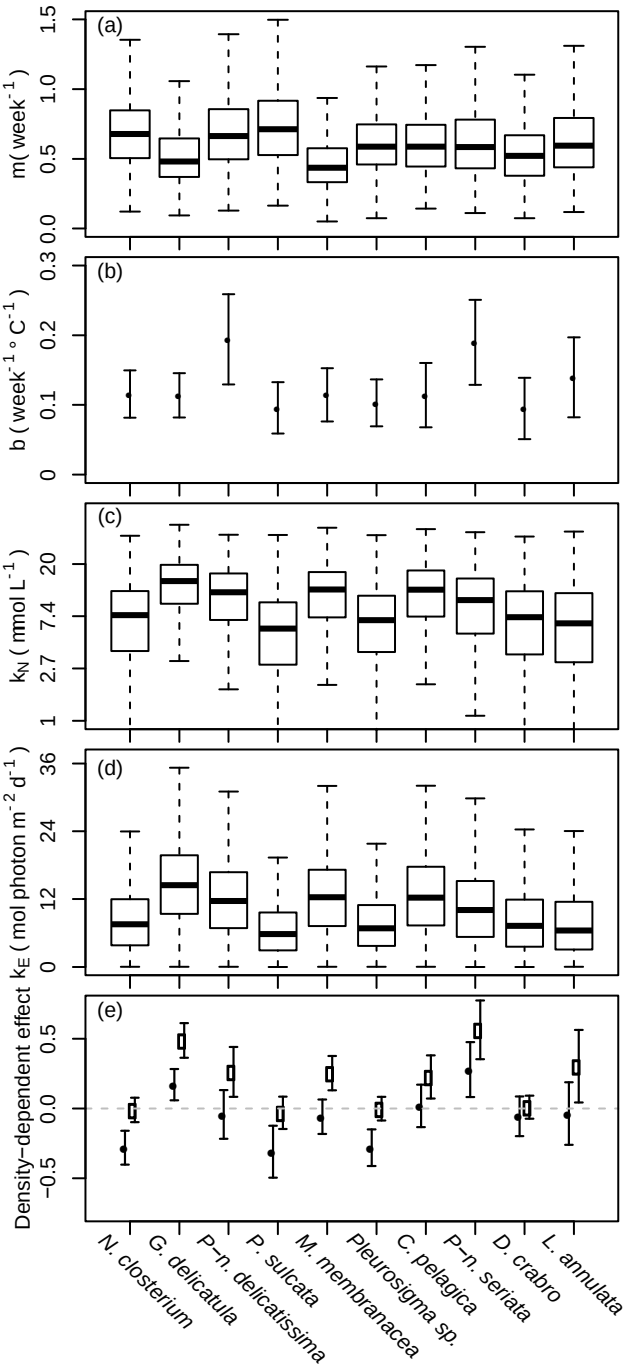
(a)
m(week^{-1})
0.0
0.5
1.0
1.5
(b)
b (week^{-1} ∘ C^{-1})
0
0.1
0.2
0.3
(c)
k_N (nmol L^{-1})
1
2.7
7.4
20
(d)
k_E (mol photon m^{-2} d^{-1})
0
12
24
36
(e)
Density−dependent effect
−0.5
0.0
0.5
N. closterium
G. delicatula
P−n. delicatissima
P. sulcata
M. membranacea
Pleurosigma sp.
C. pelagica
P−n. seriata
D. crabro
L. annulata

Table 1.

Key symbols for data and traits in the models. Traits for diatom species (as opposed to functional types) have a superscript *S* added.

Symbol	Units	Interpretation
Y_i , y_i	mg C m^{-3}	Biomass, log biomass of functional types or species in week *i*
T_i	°C	Temperature in week *i*
N_i	mg N m^{-3}	Total inorganic N in week *i*
PAR_i	mol m^{-2} d^{-1}	Sea-surface irradiance in week *i*
μ, μ^S	week^{-1}	Maximum net growth rate for a functional type, species
r, r^S	week^{-1}	Realized net growth rate for a functional type, species
k_N, k_N^S	mg N m^{-3}	Half-saturation constant for growth as a function of N concentration
k_E, k_E^S	mol m^{-2} d^{-1}	Half-saturation constant for growth as a function of irradiance
β, β^S	week^{-1} °C^{-1}	Magnitude of linear increase in net growth rate with temperature, temperature sensitivity
θ, θ^S	°C	Temperature with maximum growth rate
α, α^S		Density dependent loss coefficient within functional type, diatom species
ϕ, ϕ^S		Density dependent loss coefficient due to other functional types, other diatom species

Literature cited

Amin S, Hmelo L, van Tol H, Durham B, Carlson L, Heal K, Morales R, Berthiaume C, Parker M, Djunaedi B (2015) Interaction and signalling between a cosmopolitan phytoplankton and associated bacteria. Nature 522:98-101

Anderson TR (2005) Plankton functional type modelling: running before we can walk? J Plankton Res 27:1073-1081

Bates SS, Garrison DL, Horner RA (1998) Bloom dynamics and physiology of domoic-acid-producing *Pseudo-nitzschia* species. NATO ASI series G ecological sciences 41:267-292

Bernard KS, Steinberg DK, Schofield OM (2012) Summertime grazing impact of the dominant macrozooplankton off the Western Antarctic Peninsula. Deep Sea Research Part I: Oceanographic Research Papers 62:111-122

Bissinger JE, Montagnes DJS, Sharples J, Atkinson D (2008) Predicting marine phytoplankton maximum growth rates from temperature: improving on the Eppley curve using quantile regression. Limnol Oceanogr 53:487-493

Boyd PW, Rynearson TA, Armstrong EA, Fu F, Hayashi K, Hu Z, Hutchins DA, Kudela RM, Litchman E, Mulholland MR (2013) Marine phytoplankton temperature versus growth responses from polar to tropical waters–outcome of a scientific community-wide study. Plos ONE 8:e63091

Calbet A, Landry MR (2004) Phytoplankton growth, microzooplankton grazing, and carbon cycling in marine systems. Limnol Oceanogr 49:51-57

Cermeño P, Marañón E, Rodríguez J, Fernández E (2005) Large-sized phytoplankton sustain higher carbon-specific photosynthesis than smaller cells in a coastal eutrophic ecosystem. Mar Ecol Prog Ser 297:51-60

Chen B, Liu H, Landry MR, Dai M, Huang B, Sune J (2009) Close coupling between phytoplankton growth and microzooplankton grazing in the western South China Sea. Limnol Oceanogr 54:1084-1097

Chuang JS, Rivoire O, Leibler S (2009) Simpson's paradox in a synthetic microbial system. Science 323:272-275

Colwell RK, Rangel TF (2009) Hutchinson's duality: the once and future niche. Proc Nat Acad Sci 106:19651-19658

de Vargas C, Audic S, Henry N, Decelle J, Mahé F, Logares R, Lara E, Berney C, Le Bescot N, Probert I, Carmichael M, Poulain J, Romac S, Colin S, Aury J-M, Bittner L, Chaffron S, Dunthorn M, Engelen S, Flegontova O, Guidi L, Horák A, Jaillon O, Lima-Mendez G, Lukeš J, Malviya S, Morard R, Mulot M, Scalco E, Siano R, Vincent F, Zingone A, Dimier C, Picheral M, Searson S, Kandels-Lewis S, Coordinators TO, Acinas SG, Bork P, Bowler C, Gorsky G, Grimsley N, Hingamp P, Iudicone D, Not F, Ogata H, Pesant S, Raes J, Sieracki ME, Speich S, Stemmann L, Sunagawa S, Weissenbach J, Wincker P, Karsenti E (2015) Eukaryotic plankton diversity in the sunlit ocean. Science 348:1261605

Denman KL, Peña MA (1999) A coupled 1-D biological/physical model of the northeast subarctic Pacific Ocean with iron limitation. Deep-Sea Res Part II-Top Stud Oceanogr 46:2877-2908

Edwards KF (2016) Community trait structure in phytoplankton: seasonal dynamics from a method for sparse trait data. Ecology. in press. doi: 10.1002/ecy.1581

Eppley RW (1972) Temperature and phytoplankton growth in the sea. Fish Bull 70:1063-1085

Fehling J, Green DH, Davidson K, Bolch CJ, Bates SS (2004) Domoic acid production by *Pseudo-nitzschia seriata* (Bacillariophyceae) in Scottish waters. J Phycol 40:622-630

Field C, Behrenfeld M, Randerson J, Falkowski P (1998) Primary production of the biosphere: integrating terrestrial and oceanic components. Science 281:237-240

Fiksen Ø, Follows MJ, Aksnes DL (2013) Trait - based models of nutrient uptake in microbes extend the Michaelis - Menten framework. Limnol Oceanogr 58:193-202

Fileman E, Cummings D, Llewellyn C (2002) Microplankton community structure and the impact of microzooplankton grazing during an *Emiliania huxleyi* bloom, off the Devon coast. Journal of the Marine Biological Association of the UK 82:359-368

Finkel ZV (2001) Light absorption and size scaling of light-limited metabolism in marine diatoms. Limnol Oceanogr 46:86-94

Finkel ZV (2014) Marine Net Primary Production. Global Environmental Change. Springer

Finkel ZV, Beardall J, Flynn KJ, Quigg A, Rees TAV, Raven JA (2010) Phytoplankton in a changing world: Cell size and elemental stoichiometry. J Plankton Res 32:119-137

Finkel ZV, Irwin AJ (2000) Modeling size-dependent photosynthesis: Light absorption and the allometric rule. Journal of Theoretical Biology 204:361-369

Finkel ZV, Irwin AJ, Schofield O (2004) Resource limitation alters the 3/4 size scaling of metabolic rates in phytoplankton. Mar Ecol Prog Ser 273:269-279

Flynn KJ, St John M, Raven JA, Skibinski DO, Allen JI, Mitra A, Hofmann EE (2015) Acclimation, adaptation, traits and trade-offs in plankton functional type models: reconciling terminology for biology and modelling. J Plankton Res 37:683-691

Furnas MJ (1990) In situ growth rates of marine phytoplankton: approaches to measurement, community and species growth rates. J Plankton Res 12:1117-1151

Furnas MJ (1991) Net in situ growth rates of phytoplankton in an oligotrophic, tropical shelf ecosystem. Limnol Oceanogr 36:13-29

Gelman A, Carlin JB, Stern HS, Dunson DB, Vehtari A, Rubin DB (2013) Bayesian data analysis. Chapman and Hall, London, England

Gentleman W, Leising A, Frost B, Strom S, Murray J (2003) Functional responses for zooplankton feeding on multiple resources: a review of assumptions and biological dynamics. Deep Sea Research Part II: Topical Studies in Oceanography 50:2847-2875

Gilks WR, Richardson S, Spiegelhalter DJ (1996) Markov Chain Monte Carlo in Practice. Chapman & Hall, London, England.

Gilks WR (2005) Markov chain monte carlo. Wiley

Gregg WW, Ginoux P, Schopf PS, Casey NW (2003) Phytoplankton and iron: validation of a global three-dimension ocean biogeochemical model. Deep-Sea Res II 50:3143-3169

Grover JP (1991) Non-steady state dynamics of algal population growth: experiments with two chlorophytes. J Phycol 27:70-79

Harris R (2010) The L4 time-series: the first 20 years. J Plankton Res 32:577-583

Healey K, Monahan AH, Ianson D (2009) Perturbation dynamics of a planktonic ecosystem. J Mar Res 67:637-666

Hood RR, Laws EA, Armstrong RA, Bates NR, Brown CW, Carlson CA, Chai F, Doney SC, Falkowski PG, Feely RA, Friedrichs MAM, M.R. L, Moore JK, Nelson DM, Richardson TL, Salihoglu B, Schartau M, Toole DA, Wiggert JD (2006) Pelagic functional group modelling: progress, challenges and prospects. Deep-Sea Res II 53:459-512

Hutchinson GE (1957) Cold spring harbor symposium on quantitative biology. Concluding remarks 22:415-427

Irwin AJ, Finkel ZV (2016) Phytoplankton functional types: a functional trait perspecitive. In: Kirchman DM, Gasol JM (eds) Microbial ecology of the ocean. Wiley

Irwin AJ, Nelles AM, Finkel ZV (2012) Phytoplankton niches estimated from field data. Limnol Oceanogr 57:787-797

Kirk JT (2010) Light and Photosynthesis in Aquatic Ecosystems. Cambridge University Press

Landry M, Hassett R (1982) Estimating the grazing impact of marine micro-zooplankton. Mar Biol 67:283-288

Laws EA (2013) Evaluation of in situ phytoplankton growth rates: a synthesis of data from varied approaches. Annual review of marine science 5:247-268

Le Quéré C, Harrison SP, Colin Prentice I, Buitenhuis ET, Aumont O, Bopp L, Claustre H, Cotrim Da Cunha L, Geider R, Giraud X (2005) Ecosystem dynamics based on plankton functional types for global ocean biogeochemistry models. Global Change Biology 11:2016-2040

Litchman E, Klausmeier CA, Miller JR, Schofield OM, Falkowksi PG (2006) Multi-nutrient, multi-group model of present and future oceanic phytoplankton communities. Biogeosciences 3:585-606

Litchman E, Klausmeier CA, Schofield OM, Falkowski PG (2007) The role of functional traits and trade-offs in structuring phytoplankton communities: scaling from cellular to ecosystem level. Ecology Letters 10:1-12

Lomas MW, Bonachela JA, Levin SA, Martiny AC 2014) Impact of ocean phytoplankton diversity on phosphate uptake. Proc. Nat. Acad. Sci. USA 111: 17540-17545.

Loureiro S, Jauzein C, Garcés E, Collos Y, Camp J, Vaqué D (2009) The significance of organic nutrients in the nutrition of Pseudo-nitzschia delicatissima (Bacillariophyceae). J Plankton Res 31:399-410

MacArthur R (1960) On the relative abundance of species. Amer Natural 94:25-36

Margalef R (1978) Life-forms of phytoplankton as survival alternatives in an unstable environment. Oceanol Acta 1:493-509

Margalef R (1997) Turbulence and marine life. Sci Mar Suppl 1 61:109-123

McKinney E, Gibson C, Stewart B (1997) Planktonic diatoms in the North-West Irish Sea: a study by automatic sampler. Biology and Environment: Proceedings of the Royal Irish Academy. Royal Irish Academy

Menden-Deuer S, Lessard EJ (2000) Carbon to volume relationships for dinoflagellates, diatoms, and other protist plankton. Limnology & Oceanography 45:569-579

Merico A, Tyrrell T, Lessard EJ, Oguz T, Stabeno PJ, Zeeman SI, Whitledge TE (2004) Modelling phytoplankton succession on the Bering Sea shelf: role of climate influences and trophic interactions in generating Emiliania huxleyi blooms 1997–2000. Deep Sea Research Part I: Oceanographic Research Papers 51:1803-1826

Montagnes DJS, Kimmance SA, Atkinson D (2003) Using Q_{10}: Can growth rates increase linearly with temperature? Aquatic Microbial Ecology 32:307-313

Moore JK, Doney SC, Kleypas JA, Glover DM, Fung IY (2002) An intermediate complexity marine ecosystem model for the global domain. Deep-Sea Res II 49:403-462

Mutshinda CM, Finkel ZV, Widdicombe CE, Irwin AJ (2016) Ecological equivalence of species within phytoplankton functional groups. Funct Ecol:in press

Mutshinda CM, O'Hara RB, Woiwod IP (2009) What drives community dynamics? Proceedings of the Royal Society of London B: Biological Sciences 276:2923-2929

Mutshinda CM, O'Hara RB, Woiwod IP (2011) A multispecies perspective on ecological impacts of climatic forcing. J Animal Ecol 80:101-107

Mutshinda CM, O'Hara, RB (2011) Integrating the niche and neutral perspectives on community structure and dynamics. Oecologia 166: 241-251.

Najdek M, Blažina M, Djakovac T, Kraus R (2005) The role of the diatom *Cylindrotheca closterium* in a mucilage event in the northern Adriatic Sea: coupling with high salinity water intrusions. J Plankton Res 27:851-862

R Core Team (2016) R: A language and environment for statistical computing. R Foundation for Statistical Computing, Vienna, Austria

Raven J, Finkel Z, Irwin A (2005) Picophytoplankton: Bottom-up and top-down controls on ecology and evolution. VIE ET MILIEU-LIFE AND ENVIRONMENT 55:209-215

Raven JA (2011) The cost of photinhibition. Physiol Plant 142:87-104

Saitoh T, Chr N, Bjornstad ON (1997) Density dependence in fluctuating grey-sided vole populations. J Animal Ecol:14-24

Sher D, Thompson JW, Kashtan N, Croal L, Chisholm SW (2011) Response of *Prochlorococcus* ecotypes to co-culture with diverse marine bacteria. The ISME Journal 5:1125-1132

Sournia A, Chretiennot-Dinet M-J, Ricard M (1991) Marine phytoplankton: how many species in the world ocean? J Plankton Res 13:1093-1099

Stoecker DK (1999) Mixotrophy among dinoflagellates. Journal of Eukaryotic Microbiology 46:397-401

Sugihara G (1980) Minimal community structure: an explanation of species abundance patterns. Am Nat 116:770-787

Thomas A, O'Hara B, Ligges U, Sturtz S (2006) Making BUGS open. R news 6:12-17

Tsai A-Y, Chiang K-P, Chang J, Gong G-C (2005) Seasonal diel variations of picoplankton and nanoplankton in a subtropical western Pacific coastal ecosystem. Limnol Oceanogr 50:1221-1231

Vallina SM, Ward B, Dutkiewicz S, Follows M (2014) Maximal feeding with active prey-switching: A kill-the-winner functional response and its effect on global diversity and biogeography. Prog Oceanogr 120:93-109

van der Ploeg RR, Kirkham M (1999) On the origin of the theory of mineral nutrition of plants and the law of the minimum. Soil Sci Soc Am J 63:1055-1062

Westberry TK, Behrenfeld MJ, Siegel DA, Boss E (2008) Carbon-based primary productivity modeling with vertically resolved photoacclimation. Global Biogeochem Cycles 22:1-18

Widdicombe C, Eloire D, Harbour D, Harris R, Somerfield P (2010) Long-term phytoplankton community dynamics in the Western English Channel. J Plankton Res 32:643-655

Williams PD, Hastings A (2011) Paradoxical persistence through mixed-system dynamics: towards a unified perspective of reversal behaviours in evolutionary ecology. Proceedings of the Royal Society of London B: Biological Sciences 278:1281-1290

Zheng L, Chen B, Liu X, Huang B, Liu H, Song S (2015) Seasonal variations in the effect of microzooplankton grazing on phytoplankton in the East China Sea. Contin Shelf Res 111:304-315